Acta Cryst. (1982). A**38**, 378–387

Anatomy of a Bragg Reflexion and an Improved Prescription for Integrated Intensity

BY A. MCL. MATHIESON

Division of Chemical Physics, CSIRO, PO Box 160, *Clayton, Victoria, Australia* 3168

(*Received* 16 *June* 1981; *accepted* 7 *January* 1982)

Abstract

Using a narrow aperture in front of a detector, the intensity distribution of a single Bragg reflexion has been determined experimentally in terms of two variables, the angular setting of the crystal and that of the detector aperture. The resultant two-dimensional distributions, corresponding to the main scan procedures, ω, ω/θ, $\omega/2\theta$, show in a direct pictorial manner the interaction of the X-ray source, the spectral composition and the mosaic (and fragment) composition of the crystal. The clarity of presentation contrasts with earlier studies where the various components were projected onto one dimension. The two-dimensional presentation allows a clearer appreciation of (*a*) the rôle of the various components of the experiment and (*b*) the significance and function of the various scan procedures, ω, ω/θ, $\omega/2\theta$, corresponding to $\sigma = 0$, 1, 2 respectively, σ being the $2\theta:\omega$ scan ratio. This study leads to a new improved prescription for the measurement of integrated intensity which is more compatible with the spatial distribution of the Bragg reflexion. It also points to the existence of an inbuilt systematic error source in the conventional prescription, only made evident as a result of the extension into the second dimension. The possibility of a different procedure for the measurement of integrated intensity – the 'slice' $\omega/2\theta$ scan – is indicated. This scan has potential advantages, one being that it would allow a more precise specification of background, hence bypassing the problem of variable truncation and leading therefore to the establishment of improved accuracy in structure factors. This study should also prove of interest for the future application and exploitation of linear and two-dimensional counters in single-crystal studies.

Introduction

The experimental procedure for the measurement of integrated X-ray intensities using a relatively wide aperture has changed remarkably little from that introduced by W. H. Bragg (1914; 1969). Superficially, it appears a simple procedure but in fact it has presented a complex, and indeed long-standing, problem of establishing meaningful measurement procedures leading to accurate structure factors. This is mainly because of the wide variety of inter-related factors involved, concerning the range of scan, the appropriate aperture, the estimation of background, the effect of truncation, *etc.* After the pioneer contributions of Furnas (1957) to the diffractometry of small crystals, there was, in the 1960s, considerable concern on the matter of ω and $\omega/2\theta$ scans for the measurement of integrated intensities, *e.g.* Alexander & Smith (1962, 1964*a*,*b*); Burbank (1964, 1965); Ladell & Spielberg (1966). Subsequently, attention was drawn to the possibility of the ω/θ scan (Werner, 1972; Denne, 1977; see also Kheiker, 1969). However, no operational comparison of the various scan procedures has apparently been attempted. It has therefore not been clear whether this last variant has the superiority claimed by its proponents over the other scan methods.

The present work was initiated in an attempt to assess the situation in respect of the different scan procedures, but developed into a rather wider study. It differs somewhat from much of the work in this area in that (*a*) it involves an experimental rather than a theoretical (modelling) approach and (*b*) it deals in this respect for the first time with the diffracted X-ray intensity as a two-dimensional distribution in crystal and detector variables rather than a one-dimensional distribution in one variable with its complex projection of the contributions from the various factors.

As a result, this study provides a direct, readily-appreciated 'picture' of the interactions of the main components of the experiment for the various scans and indicates simple but convenient steps for assessing these components, thus providing information which should be useful for the overall planning of data collection on a specific crystal. The experimental results presented here are more detailed than the two-dimensional distributions derived by Einstein (1974) for the $\omega/2\theta$ scan using a mathematical modelling procedure.

This examination also reveals a possible different procedure for the measurement of integrated intensity with in-built potential for improved accuracy.

The two-dimensional mode of viewing the intensity distributions of Bragg reflexions should be of value in

0567-7394/82/030378-10$01.00

the application of position-sensitive X-ray detectors (proportional counter and photodiode types) to single-crystal diffractometry.

Experiment and results

For this experiment, it is convenient to have a symmetrical slit system with a controllable aperture in front of the scintillation detector, the height of the slit being effectively unrestricted. A small crystal* was mounted and a low-order ($\theta \sim 10°$) intense reflexion selected. This gives the reflexion reference values, ω_0, $2\theta_0$. The source was a semi-micro-focus X-ray tube, the radiation, Mo. The set-up was basic, involving only source, crystal and detector, no β-filter, no crystal monochromator. It is shown in diagrammatic form in Fig. 1 with the source (exaggerated dimensionally), the crystal and the slit/detector combination.

For a given ω setting, readings of intensity were made at a series of small offset steps (0·01°) of the 2θ axis, using as fine a slit (*ca* 0·1 mm, approximately equivalent to 0·02° in the present case), as gave an adequate count rate on the peak of the reflexion.† This procedure was repeated for a series of ω steps (0·01°) with sufficient total angular range in both ω and 2θ to reach well into the background region.

Fortuitously, in the present experiment, the crystal consisted of several slightly-misoriented fragments. While not an essential component of the exercise, consideration of their presence is instructive.

The results consist of intensity values, $I(\omega,2\theta)$, at the points of a two-dimensional array with 0·01° subdivisions in ω and 2θ. These data did not involve any correlated movement of the detector with that of the crystal and therefore correspond to the ω scan, *i.e.* $\sigma = 0$, where σ:1 is the linkage ratio between the angular displacement of the detector arm to that of the crystal. A useful way of displaying the distribution is in contour form, Fig. 2(*a*), based on a right-angled coordinate system with the crystal rotation, ω, vertical and the detector-aperture offset position, 2θ, horizontal.

While other experiments could be carried out to provide additional sets of data for ω/θ ($\sigma = 1$) and $\omega/2\theta$ ($\sigma = 2$) scan procedures using the appropriate linkage between the detector and crystal axes and repeating these scans with the 2θ shaft offset by increasing amounts, we can, in fact, use the original data set to simulate such sets by relatively simple manipulations. To do so, we have to recognize that, in a scan procedure, the detector-aperture offset position 2θ is increased by an additional $+\sigma\omega$ for each ω step of the crystal rotation axis so that the detector aperture moves across the field of Fig. 2(*a*) at an angle of arctan $(1/\sigma)$ to the horizontal (2θ) axis (assuming equi-axial subdivision). In other words, to reproduce the operation of the scan and place the appropriate intensity in the detector aperture, the row of data at $\omega_0 + \omega$ in Fig. 2(*a*) has to be moved in the *negative* 2θ direction by $\sigma\omega$ relative to the row of data at ω_0. This maintains the aperture offset position at a constant 2θ value. (The actual 2θ dial reading is, of course, $2\theta_0 + 2\theta + \sigma\omega$ when the corresponding ω dial reading is $\omega_0 + \omega$.)

Thus, from the original set of data, corresponding to the ω scan, Fig. 2(*a*), the distributions for the ω/θ scan, Fig. 2(*b*), and the $\omega/2\theta$ scan, Fig. 2(*c*), can be produced.

The main peaks in the maps, the highest being >9000 counts s^{-1} are contoured in intervals of 1000 counts s^{-1}, while the lower regions are contoured in intervals of 200 counts s^{-1}, starting at 200 and going to 1000 counts s^{-1}. Contours at 1200, 1400 and 2500 counts s^{-1} are given as dashed. These latter contours are not completed around the main peaks to avoid crowding of contour lines and consequent lack of clarity.

Interpretation

The contour maps in Fig. 2, derived solely from experiment, provide a visual summary of the interaction of the components of the experiment, the X-ray source, its spectral composition and the morphology of the crystal.

To identify the individual contributions let us consider the information contained in the maps. We deal with the various items under the headings of the three scans studied.

1. *ω scan* ($\sigma = 0$)

(i) *Crystal.* Consider a traverse, with a fine vertical slit, from A to A', Fig. 2(*a*). By the presence of the fine

* The specimen used was a crystal of cubic BN, kindly supplied by Dr R. M. Chrenko, of the Research and Development Center, General Electric Company, Schenectady, NY 12301, USA.

† (1) This measurement sequence is equivalent to the data which would be derived virtually simultaneously with a linear detector of similar spatial resolution. (2) This is effectively what Furnas (1957) designated his 'counter' scan. With a fixed $\omega/2\theta$ gear linkage, he had to use an appropriately modified procedure to effect this scan.

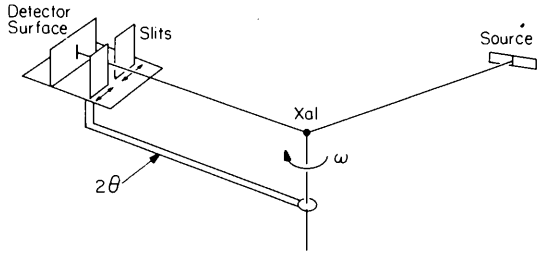

Fig. 1. The experimental arrangement with the source, the crystal and the slit/detector combination.

slit one has established that only radiation of wavelength λ_{α_1} (say) from one point of the source, Fig. 1, will be acceptable *via* the crystal and that flux will be transmitted only if a crystal fragment is at the appropriate angle to satisfy the diffraction condition. So the scan AA' reveals whether the crystal consists of one or more fragments and gives an estimate of the mosaicity of the crystalline fragments convoluted with minor contributions from other components of the experiment.*

* The magnitude of the contribution from a given component to a given line scan depends upon the orientation of the distribution for that component to the line in the particular two-dimensional distribution considered. Thus, in Fig. 2(*a*), contributions to the line scan AA' from the source and wavelength distributions are minor, whereas that from the crystal fragment/mosaicity distribution is the major one.

Fig. 3(*a*) corresponds to the section AA' and reveals the crystal specimen to consist, for this reflexion, effectively of one large fragment and three smaller fragments.

(ii) *Source.* If one considers the basic model in Fig. 1, then it is evident that, when any crystal fragment reaches the appropriate value of ω to activate reflexion of λ_{α_1} (say) from the edge of the source, traverse across the source involves a 1:1 relation of ω and 2θ. BB' in Fig. 2(*a*) therefore indicates the interaction (convolution) of the spatial distribution of the source with the effective mosaicity of the crystal and the α_2 component of the spectrum. (Choice of α_2 rather than α_1 avoids the intrusion of asymmetric fragment components.)

(iii) *Spectral components.* The wavelength component λ_{α_2} reproduces the distribution corresponding to that due to λ_{α_1}, but displaced in ω by $\theta_{\alpha_2} - \theta_{\alpha_1}$ and in 2θ by $2(\theta_{\alpha_2} - \theta_{\alpha_1})$. CC' indicates the distribution of spectral components in Fig. 2(*a*).

The essential features of the various items in the ω scan are that the distribution of the crystal fragment/mosaicity extends parallel to the ω axis, that of the source at $\sim+45°$ (arctan 1/1) to the 2θ axis (based on equi-scalar axes) and that of the spectral components at $\sim+26{\cdot}7°$ (arctan 1/2) to the 2θ axis. These are summarized in diagrammatic form for a single-component crystal in Fig. 4(*a*), both for a lower-order and a higher-order reflexion for the case of an $\alpha_1\alpha_2$ doublet. In Fig. 4, the distribution of crystal fragments (mosaic components) is depicted as symmetric, whereas the distribution for the specimen studied was asymmetric, Fig. 2.

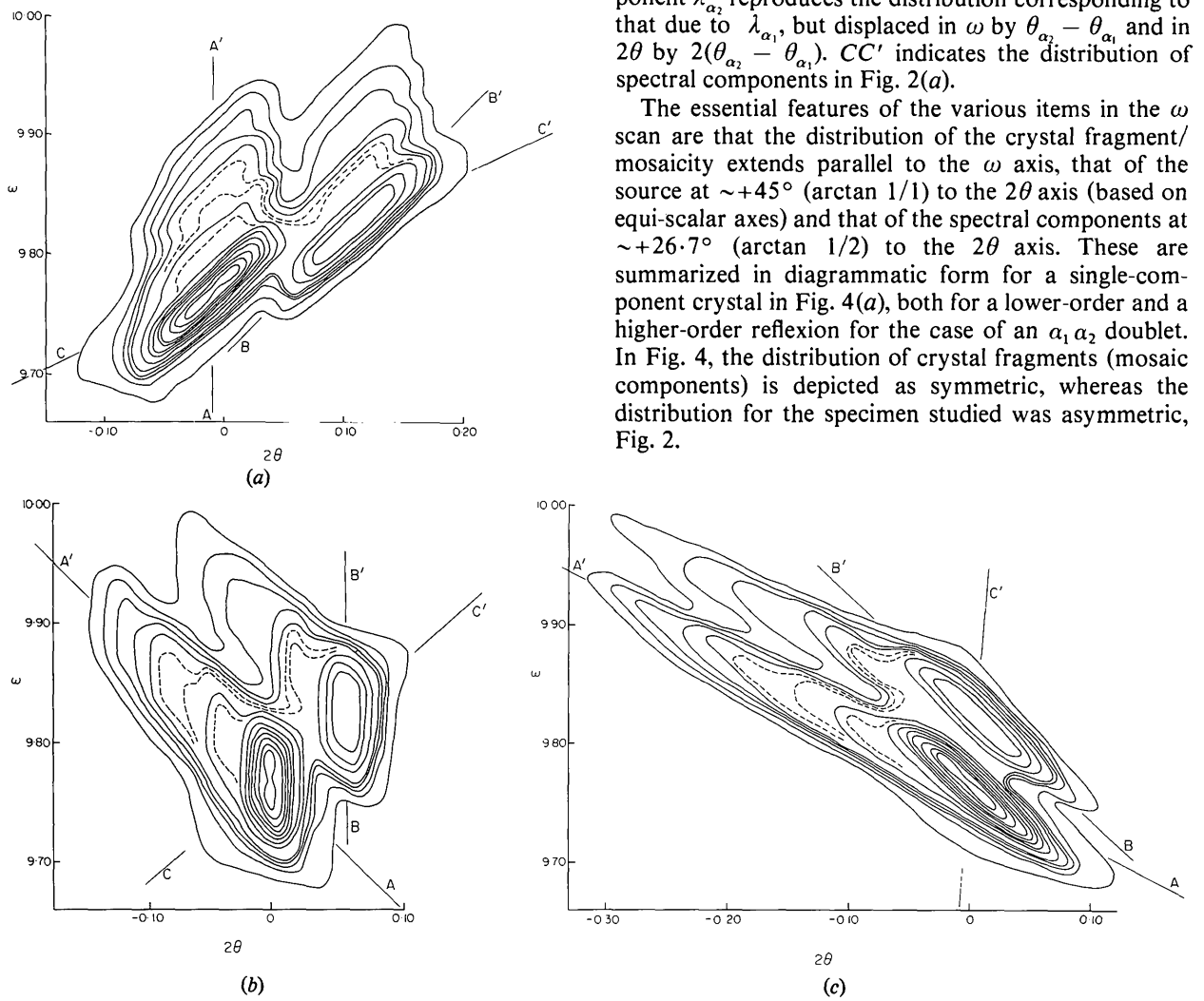

Fig. 2. The two-dimensional distribution of intensity in the Bragg reflexion, in terms of two variables, the crystal rotation , $\omega_0 + \omega$, and the detector rotation, $2\theta_0 + 2\theta + \sigma\omega$. The distributions, $I(\omega,2\theta)$, in contour form, correspond to (*a*) the ω scan ($\sigma = 0$), (*b*) the ω/θ scan ($\sigma = 1$) and (*c*) the $\omega/2\theta$ scan ($\sigma = 2$). In each case, the origin of the offset 2θ ordinate is associated with the centre of the peak of the α_1 component. The lines AA', BB', CC' correspond to the trends associated with crystal mosaic and fragment character, the source distribution and the spectral distribution respectively.

2. *ω/θ scan** ($\sigma = 1$)

(i) *Source.* Again consider a traverse with a fine slit along BB' in Fig. 2(*b*). In this case, the slit/detector combination is rotated an angle, ω, equal to that by which the crystal is moved. The combination of crystal/slit/detector moves as one and reacts only to one wavelength, such as λ_{α_1} (say). So a line parallel to the ω axis maps the source emissivity and thus provides an estimate, in angular measure, of the size of the source. Fig. 3(*b*) corresponds to this section BB'. Allowing for the crystal mosaicity, this peak width corresponds to ~0·06° in the present case. Since the source-to-crystal distance is ~200 mm, this gives the source size as 0·5 mm.

(ii) *Spectral components.* As before, the λ_{α_2} component reproduces the distribution corresponding to that due to λ_{α_1}, being displaced in ω by $\theta_{\alpha_2} - \theta_{\alpha_1}$ and in the detector aperture position by the *same amount*. The line CC' in Fig. 2(*b*) shows the distribution of spectral components.

(iii) *Crystal.* In this scan the crystal fragments (and the mosaicity) are distributed in a direction at ~45° to the -2θ axis. Again the components each image the source, AA' depicting the trend.

The essential features of the items in the ω/θ scan are that the distribution of the crystal fragment/mosaicity lies at ~−45° to the 2θ axis, that of the source is parallel to the ω axis and that of the spectral components at ~+45° to the 2θ axis. These are summarized in diagrammatic form in Fig. 4(*b*).

3. *$\omega/2\theta$ scan* ($\sigma = 2$)

(i) *Spectral components.* Consider a traverse, CC', with a fine slit, Fig. 2(*c*). Now, however, the slit/detector

* The first comment concerning this scan in diffractometry was by Furnas (1957). He referred to it as the 'source' scan.

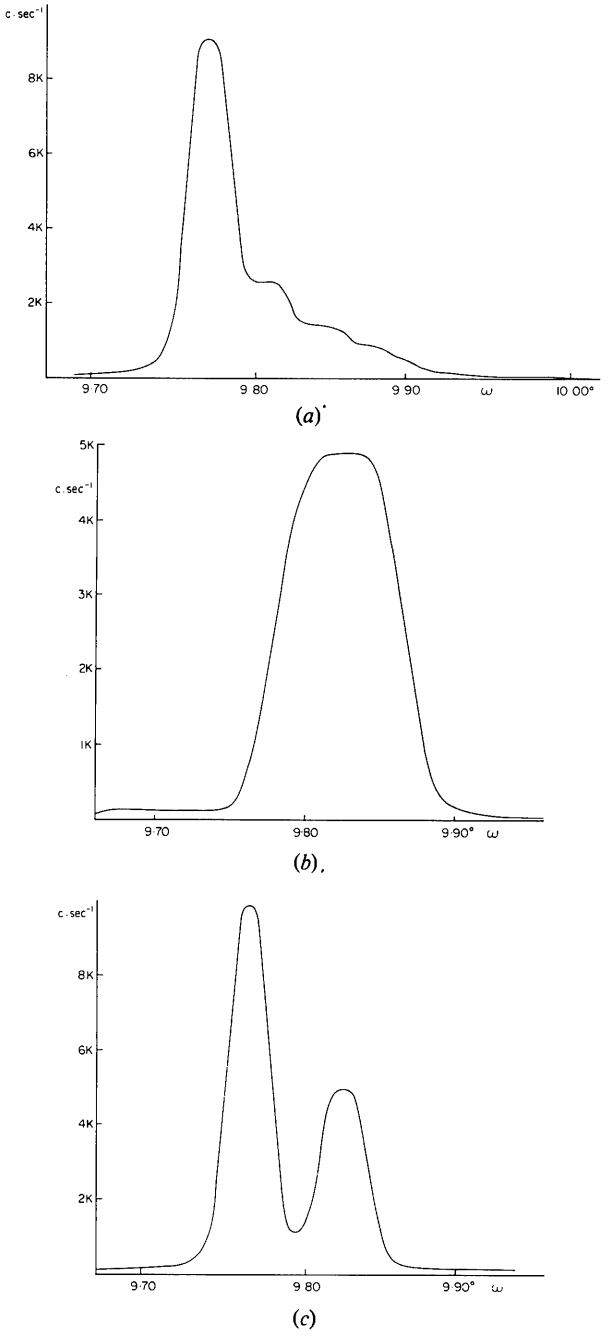

Fig. 3. These correspond to the diagnostic sections in Fig. 2. (*a*) AA' in Fig. 2(*a*), (*b*) BB' in Fig. 2(*b*), (*c*) CC' in Fig. 2(*c*). BB' is drawn through the α_2 rather than the α_1 component to minimize intrusion of the effects of crystal components.

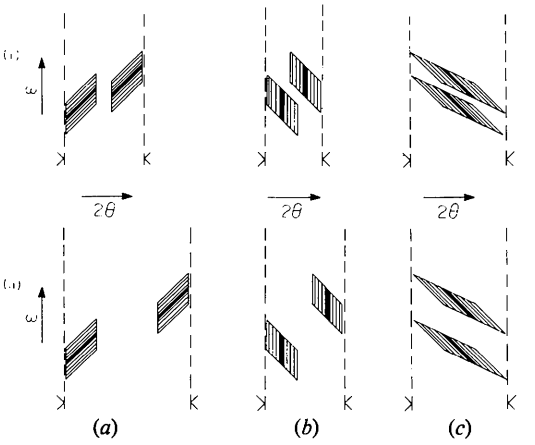

Fig. 4. Diagrammatic representation of the two-dimensional distribution of intensity in a Bragg reflexion (i) for a lower-order reflexion and (ii) for a higher-order reflexion, showing $\alpha_1\alpha_2$ doublet components in each case. The different scans are represented in (*a*) ω, (*b*) ω/θ and (*c*) $\omega/2\theta$. Two ranges of mosaicity are indicated, the narrow one by the black band and the wider one by the parallel lines within the parallelograms. The appropriate sizes of receiving apertures are indicated: that for the larger mosaicity by dashed lines with wide spacing, while for the smaller mosaicity dotted lines are used. The necessary changes in aperture on moving to a higher-order reflexion are indicated.

combination is rotated an angle, 2ω, twice that by which the crystal is rotated, ω. That is, the spectral components, (say) α_1 and α_2, Fig. 3(*c*), are displaced in the 2θ dimension so as to land in the same relative position *in the aperture.** In other words, the spectral components which pass through the slits whatever the aperture size are emitted from the *same part of the source.*

The essential features of the items in the $\omega/2\theta$ scan are that the distribution of the spectral components lies parallel to the ω axis, that of the source distribution at $\sim -45°$ to the 2θ axis, BB', and that of the crystal fragments at $\sim -26{\cdot}7°$ to the 2θ axis, AA'. These are summarized in diagrammatic form for a single-component crystal in Fig. 4(*c*).

This section has dealt with the use of a narrow aperture for diagnostic tests on the components of the experiment. Let us turn to consideration of the measurement of integrated intensity.

Conventional scan procedures – comparison

In this section, we deal with classical scan procedures using a relatively large aperture.

Let us observe first that all three contour maps in Fig. 2 (and the 2D array of point values from which they were derived) contain *in toto* the same information. The only difference is that of spatial presentation. So, given that the aperture is large enough to encompass the main intensity distribution of the peaks in Fig. 2, the main peak of the scan profile, $I(\omega)$, will have the same shape irrespective of the scan procedure chosen. It is in respect of the background that the choice of scan, its range and the choice of aperture size can differ and hence influence significantly the resultant estimate of integrated intensity.

Let us examine in some detail the process of measuring integrated intensity with a largish aperture. The process of measurement involves the addition (integration), for a given value of ω, of all the 2θ intensity values that lie between the outer limits of the chosen aperture, P_1P_2, see Fig. 5. That operation yields one point of the conventional integral scan, $I(\omega)$. Repetition at other values of ω then yields a complete set of point values and hence the integrated intensity, *i.e.* $\int_{\omega_1}^{\omega_2} I(\omega)\,d\omega$, Fig. 5.1(*a*)(ii). The normal procedure followed is to establish (arbitrary) limits such as ω_1 and ω_2 at which estimates of background are made and subtracted appropriately from the integral scan value.

In terms of our contour maps, then, the integration over the aperture is visualized as starting at some low value, ω_1, traversing vertically in Fig. 2(*a*) (say) and sampling the integral of the distribution until it reaches some upper limit, ω_2. Inspection of Figs. 2 and 4 shows clearly that the different scans explore different areas of the background region. Thus, Figs. 2(*a*) and 4(*a*) show

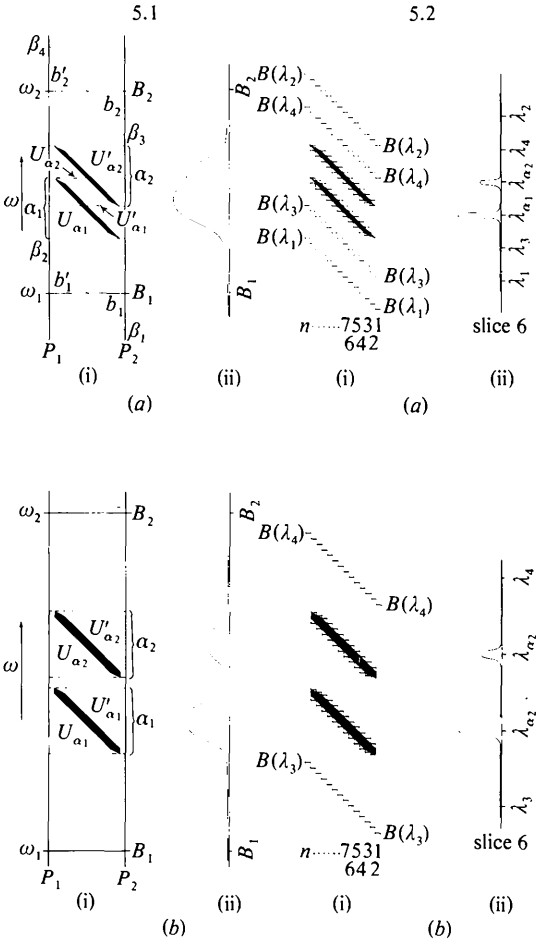

Fig. 5.1. The conventional $\omega/2\theta$ scan for the measurement of integrated intensity, involving an $\alpha_1\alpha_2$ doublet. (*a*)(i) The two-dimensional intensity distribution depicted with the receiving aperture P_1P_2. $\omega_1(B_1)$ and $\omega_2(B_2)$ correspond to the scan limits at which estimates of background intensity are conventionally made. $\beta_1\beta_2\beta_3\beta_4$ are alternative background lines (non-physical in this context) which lie parallel to the main ridge of the distribution. (*a*)(ii) The intensity profile corresponding to the conventional scan. (*b*)(i) and (ii) The equivalent components for a higher-order reflexion are depicted, showing the effect of increasing dispersion. 5.2. The slice $\omega/2\theta$ scan for the measurement of integrated intensity. (*a*)(i) The same distribution as in Fig. 5.1(*a*) divided into a series of slices by use of an aperture of limited size. $B(\lambda_n)$ correspond to limits at which background estimates can be made. Different scan ranges $\lambda_1\lambda_2$ and $\lambda_3\lambda_4$ are indicated. (*a*)(ii) The intensity profile for a typical slice. (*b*)(i) and (ii) Again the situation for a higher-order reflexion is depicted.

* This conclusion appears at first paradoxical [and indeed was not recognized explicitly in Werner's (1972) theoretical treatment, see his Fig. 4]. However, if one examines Figs. 2 and 4 in the present paper, one sees that as ω advances, α_1 first appears on the right-hand side of the detector dimension and then as it crosses the source (Fig. 1), the diffracted beam moves to the left-hand side of the detector dimension fading in intensity as it reaches the source limit. Meanwhile, the α_2 component is going through the same sequence at a slightly larger value of ω but within the same detector dimension limits.

that, for the ω scan, the traverse in ω reveals the contributions from the tails of the mosaic spread of the crystallites whereas Figs. 2(*b*) and 4(*b*) indicate that the ω/θ scan primarily examines emission from the wings of the X-ray source. Figs. 2(*c*) and 4(*c*) show that the backgrounds for the $\omega/2\theta$ scan primarily give an estimate of the radiation, other than the main wavelengths α_1, α_2, which contributes to the scan intensity. From this examination, it is obvious that there is not necessarily a unique choice as to the best scan procedure. One needs to determine which component of the experiment is providing the 'worst' background and then choose appropriately, if one is using only a single scan procedure.* To establish this matter in an individual case requires careful examination of the $I(\omega,2\theta)$ distributions outside the main intensity region. In the present case, such an examination indicates that our main background contribution comes from 'white' radiation adjoining $\alpha_1\alpha_2$ so that the $\omega/2\theta$ procedure would be most appropriate. In other cases, a different choice might be advisable.

Let us now consider briefly the question of the size of the aperture. Again, Figs. 2 and 4 should be considered. For the ω scan, the required aperture must encompass the size of the source and the spectral dispersion, $2(\theta_{\alpha_2} - \theta_{\alpha_1})$, but is independent of the mosaic (or fragment) spread. Obviously the aperture must be adjusted continuously to accommodate the changing spectral dispersion with θ.

For the ω/θ scan, the required aperture is dependent on the mosaic (fragment) spread and on the spectral dispersion, but, for the latter, only to half the extent required with the ω scan, *i.e.* $\theta_{\alpha_2} - \theta_{\alpha_1}$. The aperture has to be enlarged correspondingly as one moves to higher θ values. It is, however, largely independent of the source size.

For the $\omega/2\theta$ scan, the required aperture is dependent on the source size and the mosaic (fragment) spread. Its dependence on 2θ is minor compared with that of the ω or ω/θ scans.*

In Fig. 4, limiting aperture sizes (dotted and dashed vertical lines) have been indicated for a crystal with limited mosaic spread (dark band) and also for one with greater mosaic spread (parallel fine lines). For the ω scan, there is no distinction. The cases of lower-order and higher-order reflexions are detailed in Fig. 4(i) and (ii) respectively. In each case, $\alpha_1\alpha_2$ doublet components are shown.

The present study indicates that it is, perhaps, inappropriate to make definitive general statements as to which scan procedure is superior or which leads to the minimum size aperture, *cf.* Werner (1972) and Denne (1977). Each specific case and its end purpose requires individual assessment.

* There may indeed be a need to use different scans for different information, *e.g.* to establish TDS in a background region with minimum contributions from other sources.

* A minor component functionally dependent on θ is associated with the crystal size. Alexander & Smith (1962, 1964*a*,*b*) and Burbank (1964) give a sin θ dependence whereas Ladell & Spielberg (1966) appear to advocate a cos θ dependence.

Discussion

1. *Scan procedures*

In providing a sound basis for small-crystal diffractometry, Furnas (1957) investigated the diagnostic possibilities of the ω/θ and the pure 2θ scan (named by him the 'source' and 'counter' scans respectively) as well as of the ω and $\omega/2\theta$ scans. Despite this beginning, there has not been a great deal of significant further experimental exploration; see, however, Denne (1977). Instead, understanding of the interaction between the various components was sought through theoretical modelling. Conclusions derived from these exercises were, of course, constrained by the basic assumptions that were built into the model. For example, Werner (1972) took as his basic criterion that 'the diffracted beam should enter the detector *on its centre line for all angular settings* φ of the crystal' (my italics). It would appear that, in the case of the $\omega/2\theta$ scan, this criterion was incompatible with the fact of the beam traverse in the detector aperture (see the footnote in the $\omega/2\theta$ scan section above) and this compatibility was a significant factor in arriving at the conclusion that the $\omega/2\theta$ scan is 'essentially never advisable'. The criterion was, of course, readily and fully compatible with the ω/θ scan, see Figs. 2 and 4. So the conclusions were, in a sense, determined by the criterion chosen.

A more serious general limitation was, one can now see, the essentially one-dimensional nature of the outcome of the modelling process, namely the intensity profile, *cf.* Alexander & Smith (1962, 1964*b*), Ladell & Spielberg (1966), and Werner (1972). Perhaps the restriction to one dimension was associated with a tacit assumption that it was sufficient to focus on 2θ or on ω but not on both because either the two parameters are linked as $\theta{:}2\theta$ by the diffraction condition or by mechanical linkage. Hence, under this view, there was no need to distinguish between the $\omega(\theta)$ variable and the 2θ offset variable nor therefore an explicit need to explore the functional dependence on the two parameters since they were not seen as other than interdependent.

That the problem was essentially more than one dimensional was indicated in equation (1) of Werner (1972) which refers to $I(\gamma,\varphi)$ $[\equiv I(2\theta,\omega)]$. However, the focus of that study was the choice of scan for the measurement of integrated X-ray intensity and the functional relationship implied in his equation (1) was not investigated in terms of the two variables. Einstein (1974) followed up this aspect and carried out model

calculations of the intensity distribution in terms of two variables. These did not delineate the interactions of the various components in any great detail, except for the change in resolution of $\alpha_1\alpha_2$ (*cf.* his Fig. 13 and our Fig. 2*c*).*

While the (one-dimensional) theoretical modelling assisted in establishing many of the essential features involved in small-crystal diffractometry, their interpretation in terms of practical experimentation was not readily obvious and it did not seem to provide the crystallographer in general with a working 'picture' by which he could deduce, relatively straightforwardly, appropriate parameters for his own requirements. As a result, he has mostly not attempted to optimize his operational conditions but rather opted to follow one or other conventional procedure.

The two-dimensional view presented here should provide the working crystallographer with a more readily comprehensible picture and thus enable him to optimize his adjustable experimental parameters. The experimental requirements being simple, it is no great problem to check out one's own equipment and establish the necessary quantitative basis for experiment design.

2. *Measurement of integrated intensity with conventional scan procedures*

The presentation of a Bragg reflexion as a two-dimensional distribution rather than a one-dimensional profile allows a clearer appreciation of the functional operation of the various components and therefore a reconsideration of the factors involved in the measurement of integrated intensity. No full discussion is attempted here, consideration being restricted to certain points regarding the $\omega/2\theta$ scan procedure.

The conventional (classical) prescription for the derivation of integrated intensity by the $\omega/2\theta$ scan is given in (1):

$$\int_{\omega_1}^{\omega_2}\int_{2\theta_1}^{2\theta_2} I(\omega,2\theta+2\omega)\,\mathrm{d}2\theta\,\mathrm{d}\omega. \qquad (1)$$

This formula focuses attention on the two main components (and operations): (1) the receiving aperture which carries out the first integration, that of the intensity diffracted over the range effectively covered by the aperture, $(2\theta_2 - 2\theta_1)_{(\gamma_R)_{\lim}}$ [see Alexander & Smith (1964*b*, 1962) for definition of $(\gamma_R)_{\lim}$]; and (2) the range of scan in ω, ω_1 to ω_2, corresponding to the second integration. The background measurements, B_1 and B_2, are estimated at ω_1 and ω_2 (assuming that the conventional procedure of background estimation is followed).* The procedure prescribed in (1) is shown in diagrammatic form in Fig. 5.1.

The present study does not imply any significant change concerning the minimum receiving aperture, $(\gamma_R)_{\min}$. The exchange between Burbank (1964) and Alexander & Smith (1964*a*) appears to have established that the relevant formula† is as given in (2), see however, Ladell & Spielberg (1966).

$$(\gamma_R)_{\min} = \gamma_x + 2\gamma_m + 2\gamma_c \sin\theta. \qquad (2)$$

The major contributing factor is generally the source size, γ_x, while γ_c is usually a minor contribution and so the required variation of receiving aperture with change in θ is of second order.

When, however, one turns to the question of the appropriate scan range, the two-dimensional picture suggests a re-assessment of the significance of the parameters usually regarded as decisive in this matter.

Following Furnas (1957), Alexander & Smith (1962) give the minimum scan in ω as

$$\Delta\omega = \gamma_x + \gamma_m + \gamma_c + \gamma_\lambda\,(= S + R\tan\theta) \qquad (3)$$

and equate this to the sum of a constant term, S, and one which is proportional to $\tan\theta$, $R\tan\theta$, namely $S + R\tan\theta$. This method of determining the scan range is widely used. The values of S and R appropriate to a given experiment are usually judged, not from numerical estimates of the individual components of (3), but from inspection of selected intensity profiles or even by guesswork. Values generally chosen have $S > R$, *cf.* typical values specified by Alexander & Smith (1964*b*); Mo $K\alpha$, $\Delta\omega = 0{\cdot}90 + 0{\cdot}50\tan\theta°$.

* (1) In these calculations [see his equation (12)], he did not include the contribution associated with the source distribution, only doing so subsequently to compute integrated intensities. As a result, his calculated distributions are less physically realistic than those derived in the present work. (2) It should be noted that, due to Einstein's choice of frame of reference and his definition of ω, what he designates as ω is different from that in the present study. Also, his definition of ω focuses attention essentially on the $\omega/2\theta$ scan procedure. For comparison of his Fig. 13 with our Figs. 2(*c*) and 4(*c*), his vertical axis should be related to our crystal rotation parameter, ω, and his horizontal axis to our detector aperture offset position, 2θ. Note that our experimental results correspond to $\theta \sim 10°$; his functions were computed for $\theta = 20, 45, 70°$. (3) The reader who wishes to compare the results derived from the two different frames of reference is advised to return to the non-correlated movement of crystal and detector depicted in our Fig. 2(*a*) and work from there.

* It is evident from inspection of Figs. 2 and 4 that other procedures, involving scan estimate, *cf.* Furnas (1957), rather than stationary estimates, and the sampling of different regions of ω, 2θ, could be used for the assessment of the background. In fact, different regions could be selected for the assessment of different contributions, *e.g.* mosaicity, TDS, spectral tails.

† The nomenclature is that used in Alexander & Smith (1962):

γ_R = angular width of the receiver aperture subtended at the crystal.

γ_c = angular width of the crystal subtended at the X-ray source.

γ_x = angular width of the X-ray source subtended at the crystal.

γ_m = angular range of mosaicity of the crystal.

γ_λ = spectral dispersion on the θ scale.

If we consider Fig. 5.1(*a*)(i), we can recognize that the integrated intensity which we properly wish to estimate corresponds to that within the parallelogram $\beta_1\beta_2\beta_3\beta_4$ and, for that, the most appropriate two-dimensional integration would involve, for the first integration, use of an aperture $\beta_1\beta_2$ (which does not correspond to any physically attainable aperture but is certainly feasible in a computer, given the two-dimensional array of intensity values) and then second integration along ω. The resultant intensity profile would be different from that derived by the normal procedure, being much sharper because it would not be smeared out by γ_λ. If, now, we consider the regions in the wings adjacent to $\beta_1\beta_2$ and $\beta_3\beta_4$, we may recognize that in those regions the intensity distribution is almost flat so that there is little distinction between background estimates $\beta_1\beta_2/\beta_3\beta_4$ and B_1/B_2 because the areas b_1/b_1' and b_2/b_2' counterbalance. So, the choice of the limits of the scan essentially depends on $\gamma_m + \gamma_c + \gamma_\lambda$ *provided* B_1,B_2 are chosen to be outside the γ_x range of the α_1 and α_2 components. One concludes therefore that the appropriate choice for S and R in $S + R\tan\theta$ is, from this viewpoint, rather different, with $S < R$.

Such a change probably does not greatly modify normal procedures for $\omega/2\theta$ scan in the higher-θ region but it could significantly contract the advisable scan range in the low-angle region.

While this re-assessment suggests the need for a change of balance in the S,R parameters of the scan range which may be of operational interest for data collection, it also focuses our attention more on γ_λ. In doing so, it may therefore assist in a clearer appreciation of the intimate relation of scan range, background and truncation, showing that the limits chosen for B_1,B_2, and generally regarded as arbitrary (see Burbank, 1964), could have greater physical significance than they have previously been accorded.

The condition for a series of measurements of different reflexions to be on a common scale is that the same incident energy spectrum must be used for all measurements. This means that, if we consistently use a section of the spectrum between λ_1 and λ_2 which encompasses λ_{α_1} and λ_{α_2} (roughly centrally), then we will ensure the necessary condition. This will in fact determine not the total integrated intensity but a defined and constant (or truncated) proportion of it. Having established that the source size is a minor factor in arriving at suitable outer limits to the scan range, in dealing with the conventional procedure, this means that these limits are more closely defined in relation to wavelengths, with only a minor constant component due to crystal mosaicity and size. With the presence of the spectral doublet, one has an internal dimensional standard, $\Delta\lambda \sim 0{\cdot}0043$ Å, whose $\Delta\theta_\lambda$ equivalent can be determined for any given reflexion. One can then select some appropriate multiple of $\Delta\theta_\lambda$, say 10–15, as the scan range.* Since the individual spectral line widths expand with increasing θ in the same way as the doublet separation, their effect is absorbed in the general multiplier. The scan range is then tied to a well-established physical parameter in the experiment, *cf.* Bridgman (1936), and satisfies the necessary condition to make comparative estimations of integrated intensity.

With the criterion of measurement between the limits λ_1 and λ_2 satisfied, one is effectively measuring an exactly truncated proportion of the total integrated intensity. So the problem of truncation – which is actually that of variable truncation – is bypassed.

3. *Measurement of integrated intensity – an improved prescription*

As shown in the previous section, the determination of integrated intensity from a small crystal is, in fact, an operation involving double integration. In the conventional procedures, this feature is obscured because the first integration effectively takes place across the receiving aperture. The total integration for the conventional $\omega/2\theta$ scan takes place within the rectangular area, (say) $n_1o_1n_4o_4$ in Fig. 6.

* Burbank (1964) has pointed out that there is not necessarily a 1:1 correspondence between an area under a Cauchy distribution and an area under a reflexion peak because of the convolutive nature of an intensity peak (referring of course to a profile). The point to be noted is that, with the effective constant factors reduced to the minor components, γ_m and γ_c, the correspondence is closer and conclusions drawn accordingly more meaningful.

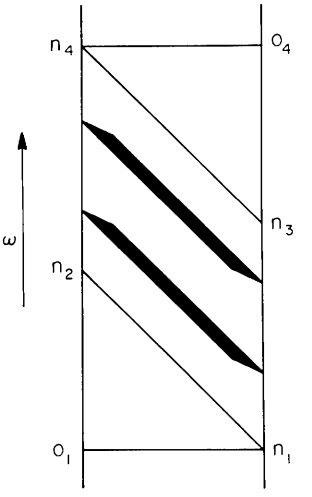

Fig. 6. Comparison of the conventional prescription for the measurement of integrated intensity with the improved prescription. The region $n_1o_1n_4o_4$ corresponds to the conventional prescription while the region $n_1n_2n_4n_3$ corresponds to the improved prescription. n_1n_3 ($\equiv n_2n_4$) corresponds to the constant energy (wavelength) bandwidth.

As we have shown, the shape of a Bragg reflexion does not, however, match such a rectangular box. Rather, it fits a parallelogram whose form depends on the scan used, *e.g.* Fig. 4. Thus, for an $\omega/2\theta$ scan, the estimation of integrated intensity should take place within an area specified (say) by the parallelogram $n_1 n_2 n_4 n_3$ in Fig. 6 or by some 'rounded' equivalent to allow for the effect of convolutive elements, *cf.* Fig. 2.

Let us imagine that we have a hypothetical highly-monochromatic X-ray spectral doublet with no wings (two Δ functions). Then integration over $n_1 o_1 n_4 o_4$ would yield the same as integration over $n_1 n_2 n_4 n_3$. If, however, the spectral source does have wings, the integration over $n_1 o_1 n_4 o_4$ will be greater than that over $n_1 n_2 n_4 n_3$ by the additional contributions $n_1 o_1 n_2$ and $n_3 o_4 n_4$. Since we require to maintain a constant spectral band to ensure comparative intensities, those two areas lie outside the band width, $n_1 n_3$ ($\equiv n_2 n_4$), and must be classified as background.

So the prescription for integrated intensity, formulated in (1), adds into the profile peak the overlap contributions, $n_1 o_1 n_2$ and $n_3 o_4 n_4$, which are strictly background. The classical prescription has, therefore, an inbuilt systematic error not, as far as I am aware, recognized or identified previously.*

This is a serious deficiency in such a basic measurement procedure, particularly for work seeking to attain the highest accuracy. It is evident that an improved prescription is needed, one which takes cognizance of the two-dimensional nature of the Bragg reflexion revealed in this study. To this end, a new prescription is formulated in (4), specifically here in respect of the $\omega/2\theta$ scan. Because the integration area is skew, an additional relationship is needed to ensure that when the reference origin $2\theta_0$ is moved to $2\theta_0 + 2\theta_s$, ω_0 is correspondingly adjusted to $\omega_0 + 2\theta_s$. This ensures that the reference point for the ω-scan range moves along the locus of the source, *cf.* Figs. 2(*c*) and 4(*c*).

$$\int_{2\theta_{s_1}}^{2\theta_{s_2}} \int_{\omega_1}^{\omega_2} I(2\theta_s + \omega, 2\theta_s + 2\theta + 2\omega)\, \mathrm{d}\omega\, \mathrm{d}2\theta_s. \qquad (4)$$

The obvious procedure to convert this prescription into a practical operation would be to carry out a point-by-point count, as in the present study, or, more expeditiously, with a linear detector of sufficient spatial resolution and, by appropriate manipulation in a computer, extract a proper estimate of the integrated intensity according to (4). As a simpler equivalent, can one devise a procedure using a standard scintillation detector – one which will allow relatively straightforward recognition (and hence exclusion or partial exclusion) of redundant areas and so yield an improved measure of integrated intensity over a normal range of θ?

One method would be to use a relatively narrow aperture and scan this in a series of steps in 2θ to traverse the distribution in slices, Fig. 5.2.*

This 'slice' scan procedure with the $\omega/2\theta$ scan has a rather useful feature, Fig. 5.2(*a*)(ii). Each slice, *cf.* Fig. 3(*c*), contains a spectrum analysis which must be essentially identical in intensity distribution for each slice, merely displaced in ω. So, each slice contains an inbuilt diagnostic, which, by inspection, or test in a computer, if on line, can establish that the individual slice measurement is acceptable.

Because of its relatively high resolution, this spectrum allows upper and lower background locations, $B_1(\lambda_1)$ and $B_2(\lambda_2)$, for each slice to be determined consistently relative to the spectral components λ_{α_1} and λ_{α_2} even to relatively low values of θ. The definition of the two background cut-off points is more clearly established in the slice-scan by contrast with the poorer definition necessarily associated with the integral scan, since convolution with the source, normally the largest contributor, is involved only minimally. So the measurement of integrated intensity is now that of the intensity diffracted between λ_1 and λ_2 which corresponds to a constant proportion of the total scan intensity, even though the actual ratio cannot be established experimentally. The measurement of the total integrated intensity is experimentally virtually impossible if any of the features of the experiment correspond to a non-Gaussian distribution, *e.g.* Cauchy. However, using λ_{α_1} and λ_{α_2} as references, we can establish λ_1 and λ_2 as background points so that relative estimates of different reflexions are directly comparable without seeking to establish a measure of the total intensities. If λ_1 and λ_2 prove to extend too far in reciprocal space in the higher-θ region, one can choose closer λ_3 and λ_4 limits more suited to the higher angles, *cf.* Figs. 5.2(*a*) and 5.2(*b*). A range of intermediate θ reflexions with backgrounds established both at $\lambda_1 \lambda_2$ and $\lambda_3 \lambda_4$ would allow for interpolation.

I would like to express appreciation of the opportunities for the exchange of views with Dr B. P. Schoenborn on the two-dimensional aspects of Bragg neutron reflexions during the period he spent in this Division. I am also grateful to my colleagues, Drs S. L. Mair and S. W. Wilkins and to an anonymous referee for critical and helpful comments on the manuscript.

* This could be another contributing factor to the 'as yet improperly-accounted-for source of error' (USA National Research Council, 1976; see also Mathieson, 1979).

* The conditions depicted in Fig. 5.2 are, of course, idealized. Initial consideration might suggest that an exact equality would be required for the size of the detector aperture and the unit size of the 'slice' in 2θ. Further consideration, however, establishes that, provided the aperture is dimensionally stable and the aperture size and unit step are comparable, the *ratio* of integrated intensities for different reflexions is sustained.

(*a*)

(*b*)

(*c*)

Fig. 7. Photographs of the distributions corresponding to the ω, ω/θ and $\omega/2\theta$ scan procedures taken by stepping a film vertically past a narrow horizontal slit mounted on the detector arm, the film steps being synchronized with the crystal steps. These correspond to magnification of the order of $\times 20$.

Postscript

While use of a narrow vertical aperture and a quantum detector gives a quantitative estimate of the two-dimensional distributions, $I(\omega,2\theta)$, corresponding to the various scan procedures, equivalent photographs of the distributions can be obtained by a simple procedure. This involves mounting a narrow *horizontal* aperture on the detector arm of the diffractometer with, behind it, a device to allow controlled vertical traverse of a small piece of X-ray film. After each exposure (in the present case ~30 s), the crystal rotation axis is displaced by a given amount, ω, the detector arm by an amount $\sigma\omega$ (corresponding to a σ scan) and the film is moved vertically by a proportional displacement, chosen so that the resultant axial subdivisions are nearly equal. This is repeated until the required range of ω has been traversed. The results of applying this procedure for ω, ω/θ and $\omega/2\theta$ scans to the same reflexion as dealt with in the main text are shown in Fig. 7 and should be compared with the corresponding contour maps in Fig. 2.

References

ALEXANDER, L. E. & SMITH, G. S. (1962). *Acta Cryst.* **15**, 983–1004.

ALEXANDER, L. E. & SMITH, G. S. (1964*a*). *Acta Cryst.* **17**, 447–448.

ALEXANDER, L. E. & SMITH, G. S. (1964*b*). *Acta Cryst.* **17**, 1195–1201.

BRAGG, W. H. (1914). *Philos. Mag.* **27**, 881.

BRAGG, W. H. (1969). *Acta Cryst.* A**25**, 3–11.

BRIDGMAN, P. W. (1936). *The Nature of Physical Theory*. New York: Dover.

BURBANK, R. D. (1964). *Acta Cryst.* **17**, 434–442.

BURBANK, R. D. (1965). *Acta Cryst.* **18**, 88–97.

DENNE, W. A. (1977). *Acta Cryst.* A**33**, 987–992.

EINSTEIN, J. R. (1974). *J. Appl. Cryst.* **7**, 331–344.

FURNAS, T. C. (1957). *Simple Crystal Orienter Instruction Manual*. Milwaukee: General Electric Company.

KHEIKER, D. M. (1969). *Acta Cryst.* A**25**, 82–87.

LADELL, J. & SPIELBERG, N. (1966). *Acta Cryst.* **21**, 103–118.

MATHIESON, A. McL. (1979). *Acta Cryst.* A**35**, 50–57.

USA NATIONAL RESEARCH COUNCIL (1976). *Status and Future Potential of Crystallography*, p. 22. Washington, DC: National Academy of Sciences.

WERNER, S. A. (1972). *Acta Cryst.* A**28**, 143–151.